HEAT BUDGET OF THE CENTRAL AMERICAN SEAS

STEFAN HASTENRATH*

RESUMEN

Se calculó el balance calórico de las áreas del Golfo de México, Corriente de Florida, Mar Caribe y Océano Pacífico Oriental, a base de observaciones de barcos durante 1911–70. La distribución de la radiación neta está dictada sobre todo por la nubosidad y la latitud geográfica. Los flujos de calor sensible y latente alcanzan sus máximos valores en el área de la Corriente de Florida y en invierno, cuando los contrastes de temperatura entre mar y aire son más pronunciados; por otra parte, los valores más bajos se encuentran en la zona de aguas frías a lo largo de la costa Norte del Continente Suramericano. Para el año entero, el océano exporta energía de 13 Watts m^{-2} del Pacífico Oriental, pero importa calor de 24, 43 y 3 Watts m^{-2} en el Golfo de México, la Corriente de Florida, y el Mar Caribe, respectivamente.

ABSTRACT

The oceanic heat budget of the Gulf of Mexico, Gulf Stream region, Caribbean Sea, and Eastern North Pacific is calculated on the basis of ship observations during 1911–70. Net radiation largely follows the pattern of cloudiness, apart from its latitudinal dependence. Latent and sensible heat flux is largest in the Gulf Stream domain during winter, when sea–air temperature contrasts are most pronounced; smallest values are found in the cold water regions along the North Coast of South America. For the year as a whole, the ocean imports heat at the rate of 24, 43 and 3 W m^{-2} in the Gulf of Mexico, Gulf Stream region, and Caribbean Sea, respectively, but exports 13 W m^{-2} from the Eastern North Pacific.

* *Department of Meteorology, The University of Wisconsin, U.S.A.*

INTRODUCTION

The atmospheric–hydrospheric energetics of the Caribbean–Gulf of Mexico region have been studied on the basis of climatic atlas data (Colón, 1963), and in more detail for a single year (Hastenrath, 1966 a, b, 1968). Budyko's (1963) atlas also covers this area. Long–term ship observations compiled in an unprecedented spatial resolution (Hastenrath and Lamb, 1977) invited a reappraisal of the oceanic heat budget. Results of these calculations are presented in this paper.

2. DATA

Ship observations taken over the tropical Atlantic and Eastern Pacific during 1911–70 were obtained from the National Climatic Center at Asheville, North Carolina, and compiled into a climatic atlas (Hastenrath and Lamb, 1977), with data being processed by one degree square areas. An atlas of the oceanic heat budget, based on the same data, and containing monthly and annual maps of the key budget terms, is in preparation. Some 3.7 million ship observations are available for the ocean area depicted in Figs. 1–4. Satellite–derived net radiation data for the top of the atmosphere averaged over a few years have been published recently (Vonder Haar and Ellis, 1974), but these refer to the middle of ten degree squares.

3. BASIC THEORY

The heat budget equation for the oceanic water body can in approximate form be written:

$$SW\uparrow\downarrow + LW\uparrow\downarrow = Q_s + Q_e + (Q_v + Q_t) \qquad (1)$$

The left–hand terms are net shortwave and longwave radiation at the ocean surface, and the right–hand terms denote sensible and latent heat flux at the sea–air interface, heat export and storage within the ocean, respectively.

For the computation of net shortwave radiation $SW\uparrow\downarrow$ a variety of empirical formulae has been suggested (e.g., Budyko, 1958), using total cloudiness C_T and latitude as input. In the present study use was made of the theoretical framework presented by Bernhardt and Philipps (1958). The net shortwave radiation at the ocean surface is the resultant of five flux components:

$$SW\uparrow\downarrow_{sfc} = SW\downarrow_{sfc} (\text{dir, clear}) + SW\downarrow_{sfc} (\text{diff, clear}) + SW\downarrow_{sfc} (\text{diff, cloudy}) + SW\uparrow_{sfc} (\text{dir}) + SW\uparrow_{sfc} (\text{diff}) \quad (2)$$

These are the downward directed direct solar radiation for the clear portion, the downward directed diffuse solar radiation for the clear and the cloudy portions of the sky, and the upward directed direct and diffuse shortwave radiation, respectively.

The downward directed direct solar radiation for the clear portion of the sky is given by Bernhardt and Philipps (1958):

$$SW\downarrow_{sfc} (\text{dir, clear}) = (1 - C_T) \frac{I_o}{\rho^2 (\delta)} \cos\theta \left[\frac{0.907}{(\cos\theta)^{0.018}} \right]^{\frac{T}{\cos\theta}} \quad (3)$$

The zenith angle θ of the sun is determined by the declination δ, the latitude ϕ, and the hour angle ω, namely

$$\cos\theta = \sin\delta \sin\phi + \cos\delta \cos\phi \cos\omega \quad (4)$$

The value for the solar constant $I_o = 1{,}352\ W\ m^{-2}$, the ratio of true to mean distance of the sun ρ, and the solar declination δ for the middle of each calendar month, were taken from List (1968).

T is the so–called "old" Linke turbidity factor. A spatially varying T by calendar month was calculated from surface specific humidity q (g/kg) according to

$$T = 1.40 + 0.136\ q \quad (5)$$

In specifying the dependence on q in Eq. (5) use was made of conventional empirical relationships between absorption and precipitable water and between precipitable water and surface humidity. For the contribution by dust the constant value of 0.40 was adopted, due to lack of information on spatial pattern and seasonal variation of dust loads over the Atlantic and Eastern Pacific (Bernhardt and Philipps, 1958; Lettau, 1939; Drs. T. N. Carlson, Pennsylvania State University, J. Prospero, University of Miami, R. Jaenicke and L. Schütz, Max–Planck Institut für Chemie, Mainz, personal communications 1976).

To obtain monthly means of $SW\downarrow_{sfc}$ (dir, clear), Eqs. (3) and (4) were applied by hourly intervals and values were then integrated over all sun angles. This was done for the middle of each calendar month and for one degree latitude strips, with a spatially varying turbidity factor according to Eq. (5).

Values of $\eta = \beta = 0.36$ were used in the calculation of $SW\downarrow_{sfc}$ (diff, clear) and $SW\downarrow_{sfc}$ (diff, cloudy). Here η is the ratio of diffuse radiation under completely cloudy to global radiation with cloudless sky; and β is the ratio of diffuse radiation to the difference between extraterrestrial radiation and direct radiation with cloudless sky. With these ratios, $SW\downarrow_{sfc}$ (diff, clear) and $SW\downarrow_{sfc}$ (diff, cloudy) were calculated using Eqs. (3) and (4). The upward directed shortwave flux components $SW\uparrow_{sfc}$ (dir) and $SW\downarrow_{sfc}$ (diff) were then computed using an albedo for the ocean surface of 6 percent (List, 1968).

$SW\uparrow\downarrow$ was computed using the above procedure, rather than that due to Budyko (1958), because it accounts for spatial variation of water vapor turbidity and would allow for varying dust turbidity as pertinent information may become available. For comparative purposes both procedures were applied to actual data, with the following results. Global radiation with cloudless sky computed using the above method is smaller than Budyko's latitude–mean values by about 15 W m^{-2}. However, variations along a latitude circle resulting from the humidity pattern are of the same magnitude, but are ignored by the Budyko procedure. For global radiation with actual cloud cover, the above method yields values only about 5–10 W m^{-2}, or a few percent, smaller than Budyko's procedure: Budyko uses a somewhat stronger

reduction of radiation due to cloudiness. Both methods assume the same value for the albedo of the ocean surface. Consequently maps of net shortwave radiation with actual cloud cover differ by a few percent. This is well within the uncertainty of either method.

Net longwave radiation was computed from Brunt's formula (Budyko, 1958):

$$LW\uparrow\downarrow = \varepsilon \sigma T_w^4 (0.39 - .056\sqrt{q}\,)(1 - 0.53 C_T^2) + 4 \varepsilon \sigma T_w^3 (T_w - T_a) \quad (6)$$

sea surface temperature T_w and air temperature T_a being in degrees K,, and surface specific humidity q in gm/kg, emissivity $\varepsilon = 1$ and Stefan–Boltzmann's constant $\sigma = 567 \times 10^{-10}$ W m^{-2} K^{-4}

Sensible and latent heat flux were calculated from the bulk–aerodynamic equations:

$$Q_s = \rho C_D c_p (T_w - T_a) V \quad (7)$$

$$Q_e = \rho C_D L (q_w - q_a) V \quad (8)$$

Values of $\rho = 1.175$ kg m^{-3} and $C_D = 1.4 \times 10^{-3}$ were used for air density and drag coefficient, respectively. c_p is specific heat at constant pressure and L latent heat of evaporation. The saturation specific humidity corresponding to the sea surface temperature T_w was computed for q_w with reference to a salinity of 35 per mille; and scalar mean wind speed was used for V.

Of the observational data mentioned in section 2, the following elements thus served as input to the heat budget calculations: total cloudiness, dew point, and pressure for SW↑↓; sea surface and air temperature, dew point, pressure, and cloudiness for LW↑↓ ; sea surface and air temperature, dew point, pressure, and scalar wind speed for Q_s and Q_e.

Calculations were performed by calendar month, using sixty–year mean data. Covariance between elements can make the product of averages differ from the average of products, and C_D depends on

stability (Bunker, 1976). However, these effects may be of subordinate importance for the low–latitude oceans mapped here. In fact, Bunker's (1976) annual maps of Q_e and Q_s for the North Atlantic are rather similar to the present charts: only in limited areas are his figures of Q_e by about 15 W m^{-2} larger than the present ones, a difference of about ten percent. However, Bunker's (1976) values of net radiation SWLW$\uparrow\downarrow$, calculated from somewhat different empirical formulae, are systematically larger than in the present study. Consequently, his residual $(Q_v + Q_t)$ differs from Fig. 4 towards larger positive values. The drag coefficient chosen here is well within the tolerance of recent empirical studies (Pond *et al.*, 1974; Ching, 1975). Annual maps of heat budget components were constructed from the sets of twelve monthly computations. All maps were machine–isoplethed and then re–drawn by hand.

4. SPATIAL PATTERNS

The annual mean map of net radiation SWLW$\uparrow\downarrow$, Fig. 1, shows some latitudinal variation, but apart from that largely follows the pattern of cloudiness. Comparatively large values are found at the margin of the North Atlantic high and in the region of lower–tropospheric divergence along the North coast of South America (Hastenrath, 1976). Net radiation is smallest in the Western Caribbean off the Central American coast and in the zonally oriented band of maximum cloudiness over the Eastern North Pacific.

Sensible heat flux at the sea–air interface Q_s, Fig. 2, is a small term in the energy budget of the tropical seas. The flux is mostly directed from ocean to atmosphere, except for the cold water region along the North coast of South America.

Latent heat flux Q_e, Fig. 3, reaches its highest values in the Gulf Stream domain, where the advection of warm waters accounts for a large sea–air temperature difference especially during winter. Evaporation is small in the cold water region along the North coast of South America.

Fig. 4 maps the sum of divergence of heat transport and storage

within the ocean ($Q_v + Q_t$) obtained as a residual. For annual mean conditions depicted here, this essentially represents the divergence of heat transport within the oceanic water body Q_v. Heat export takes place from much of the area, but import is indicated for the higher latitude portions of the map, in particular the realm of the Gulf Stream system. Comparison with satellite–derived net radiation estimates for the top of the atmosphere (Vonder Haar and Ellis, 1974), suggests that oceanic export/import contributes substantially to the heat balance of the atmosphere–hydrosphere system (Table 1).

5. SEASONAL MARCH

The seasonal variation of the major heat budget components is displayed in Figs. 5–8 for four representative sea areas as identified in Fig. 4, by straight dotted lines namely Gulf of Mexico, Gulf Stream domain, Caribbean Sea and Eastern North Pacific.

Consistent with the subtropical latitude of the Gulf of Mexico, the annual range of net radiation is comparatively large (Fig. 5). The exchange of latent and sensible heat is most intense during fall and winter, when sea–air temperature contrasts are most pronounced. The sum of divergence of heat transport and storage within the water body ($Q_v + Q_t$), obtained as a residual is positive in spring and summer, reaches the largest negative values in late fall and early winter, and indicates an import of heat for the year as a whole. Net radiation, plotted in Fig. 5 has a somewhat larger annual mean and smaller range than Hastenrath's (1968) earlier estimates. The ($Q_v + Q_t$) obtained here as a residual is similar to the earlier estimates by direct calculation (Hastenrath, 1968).

Heat budget characteristics in the Gulf Stream domain, to the East of Florida (Fig. 6) are similar to the Gulf of Mexico, except for the larger evaporation and the larger heat import within the oceanic water body.

For the Caribbean Sea (Fig. 7) net radiation has a larger annual mean and smaller range than for the Gulf of Mexico. Mean and seasonal variation of the sensible and latent heat fluxes are also much reduced. The residual ($Q_v + Q_t$) has a similar though much smaller seasonal

variation as in the Gulf of Mexico, with a near zero heat import resulting for the annual mean. In comparison to earlier estimates for the Caribbean Sea (Colón, 1963; Hastenrath, 1968), the annual mean of net radiation arrived at in the present study is somewhat smaller, while the residual ($Q_v + Q_t$) is similar.

The area of the Eastern North Pacific depicted in Fig. 4 and 8 is at the same latitude as the Caribbean Sea (Fig. 6), and the heat budget terms have a similar magnitude, though less distinct seasonal march. The ocean exports heat from this region for the year as a whole.

6. CONCLUSIONS

Evaluation of long–term ship observations allowed a mapping of the key oceanic heat budget components in greater spatial detail than had so far been available (Budyko, 1963). The pattern of net radiation is largely dictated by cloudiness, apart from the broad latitudinal control. The major features in spatial and temporal distribution of the sensible and latent heat flux can be understood from the pattern of sea–air temperature difference, in that the largest heat exchange is found in the higher latitudes during winter.

From a comparison with earlier calculations the error in net radiation (SW + LW)↑↓ is estimated to be about 10–20 W m^{-2}, or around ten percent. The error in estimating the sum of sensible and latent heat flux ($Q_s + Q_e$) is primarily related to uncertainties in the drag coefficient C_D. This error may be of the order of ten percent, or about 10–15 Wm^{-2}. Accordingly, the residual sum of divergence of heat transport and storage within the oceanic water body may be in error by about 20–30 W m^{-2}. With this reservation, the ocean imports heat in the realm of the Gulf of Mexico and the Gulf Stream, with export indicated for much of the lower–latitude portions of the map area. A comparison with satellite–derived estimates of net radiation at the top of the atmosphere (Table 1) indicates that the oceanic water body in part of this region contributes a sustantial share to the redistribution of energy to other parts of the globe.

ACKNOWLEDGEMENTS

This study was supported by the Office for Climate Dynamics of the National Science Foundation. P. Lamb and P. Guetter did the computer programming.

Table 1. Ratio of annual mean divergence of heat transport and storage within the ocean to net radiation at the top of the atmosphere, $(Q_v + Q_t)/SWLW\uparrow\downarrow_{top}$, in percent.

	110–100 W	100–90	90–80	80–70	70–60	60–50
30–20 N	–	–50	–108	–120	–52	–14
20–10	+10	–	–	– 5	+11	–25
10– 0	+ 9	– 8	+ 21	–	–	–

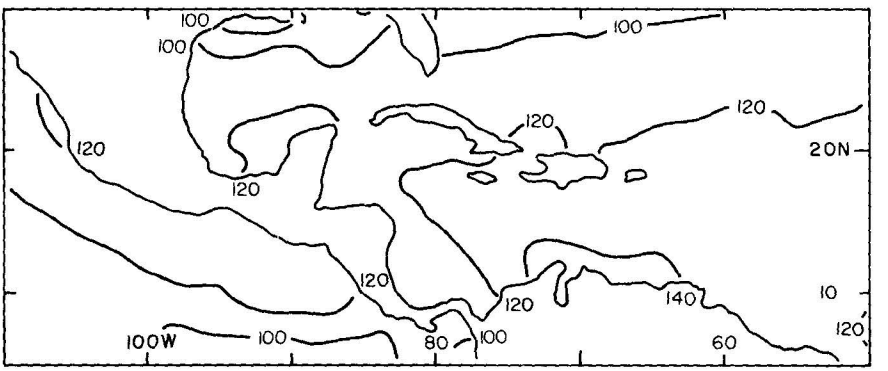

Fig. 1. Annual mean net radiation at the ocean surface, SWLW$\uparrow\downarrow$ in W m^{-2}.

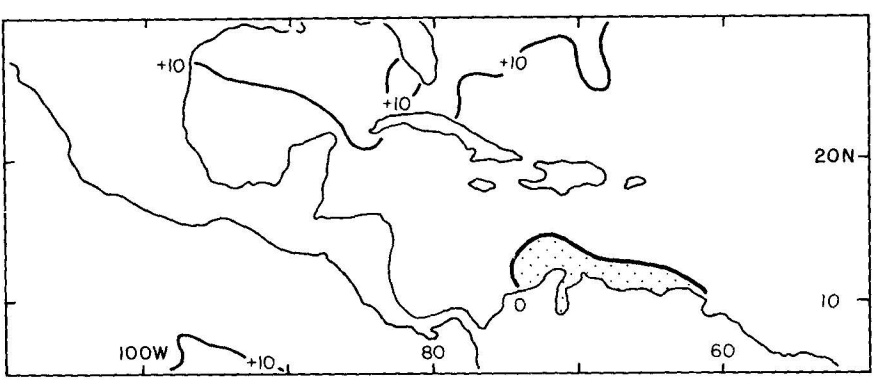

Fig. 2. Annual mean of sensible heat flux, Q_s, in W m^{-2}. Stippling denotes areas of downward directed heat flux.

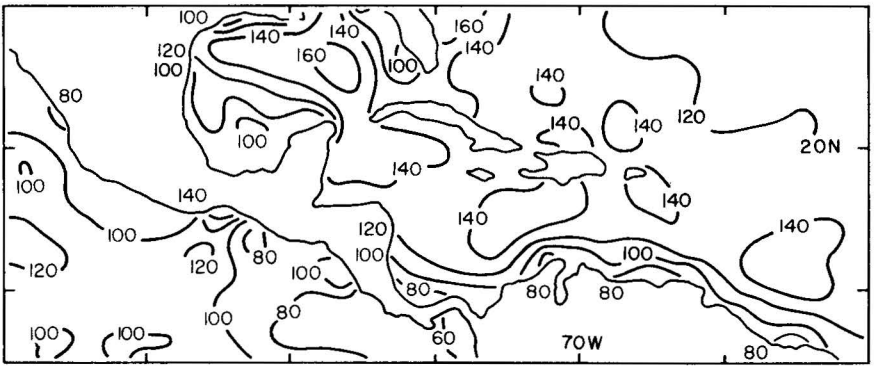

Fig. 3. Annual mean of latent heat flux Q_e, in W m^{-2}.

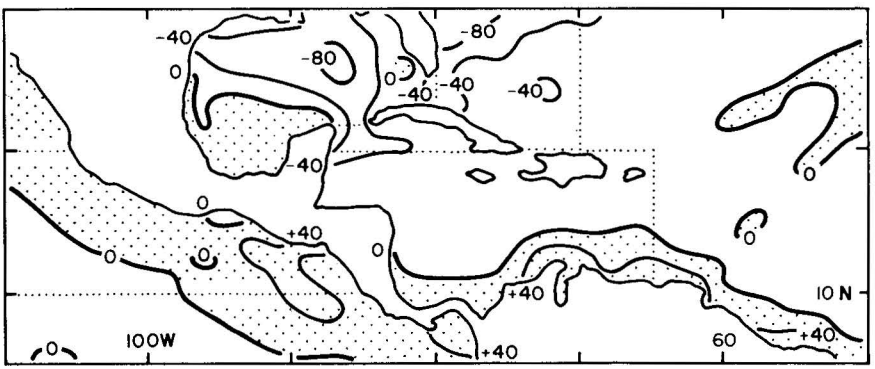

Fig. 4. Annual mean of divergence of heat transport and storage within the ocean $(Q_v + Q_t)$, obtained as residual, in W m^{-2}. Stippling denotes areas of heat export. Dotted rectangles indicate areas referred to in Figs. 5-7.

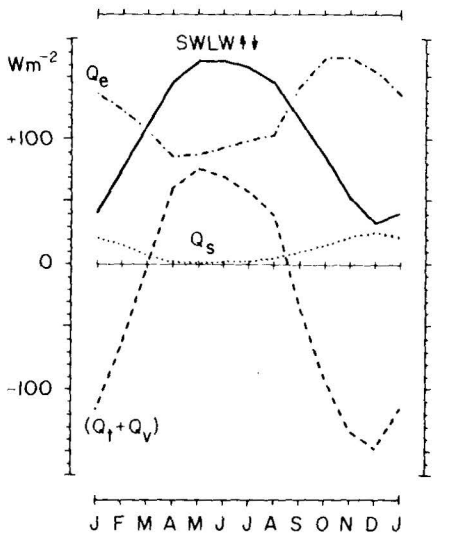

Fig. 5. Gulf of Mexico. Seasonal march of heat budget components. Solid, dotted, dash-dotted, and broken lines denote net radiation (SWLW↑↓), sensible Q_s and latent heat flux Q_e, and the sum of divergence of heat transport and storage within the oceanic water body ($Q_v + Q_t$), obtained as residual.

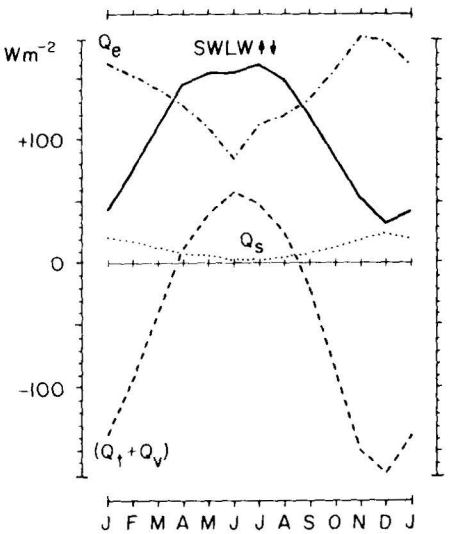

Fig. 6. Gulf Stream domain. Seasonal march of heat budget components. Symbols as in Figs. 5-6.

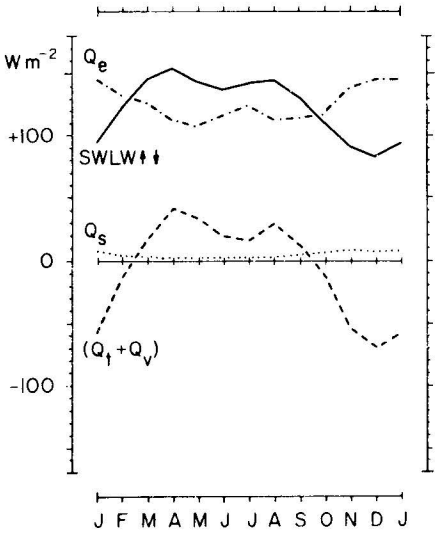

Fig. 7. Caribbean Sea. Seasonal march of heat budget components. Symbols as in Fig. 5.

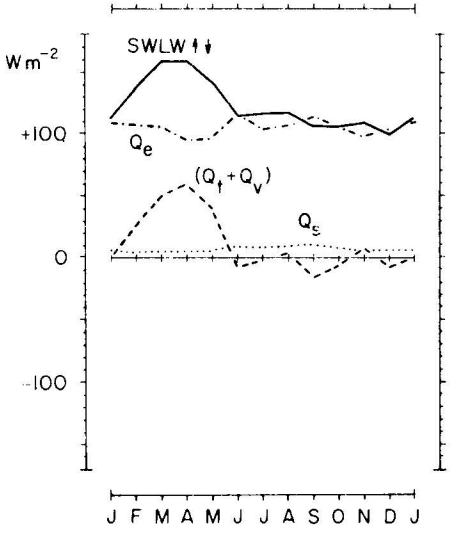

Fig. 8. Eastern North Pacific. Seasonal march of heat budget components. Symbols as in Figs. 5-7.

BIBLIOGRAPHY

BERNHARDT, F., H. PHILIPPS, 1958. Die raumliche und zeitliche Verteilung der Einstrahlung, der Ausstrahlung, und der Strahlungsbilanz im Meeresniveau. I. Die Einstrahlung.
Abhandlungen Meteorol. Hydrol. Dienst. DDR, No. 45, Akademie–Verlang Berlin, 227 pp.

BUDYKO, M. I., 1958. The heat balance of the Earth's surface. English translation by U. S. Weather Bureau, Washington, D. C.

BUDYKO, M. I., 1963. Atlas of the heat balance of the Earth (in Russian), Kartfabrika Gosgeoltehizdata, Leningrad.

BUNKER, A., 1976. Computations of surface energy flux and annual air–sea interaction cycles of the North Atlantic Ocean. *Mon. Wea. Rev.*, 104, 1122–1140.

CHING, J. K. S., 1975. Determining the drag coefficient from vorticity, momentum, and mass budget analyses. *J. Atm. Sci.*, 32, 1898–1908.

COLON, J. A., 1963. Seasonal variations in heat flux from the sea surface to the atmosphere over the Caribbean Sea. *J. Geophys. Res.*, 68, 1421–1430.

HASTENRATH, S., 1966 a. On general circulation and energy budget in the area of the Central American Seas. *J. Atm. Sci.*, 23, 694–711.

HASTENRATH, S., 1966 b. The flux of atmospheric water vapor over the Caribbean Sea and the Gulf of Mexico. *J. Appl. Meteor.*, 8, 778–788.

HASTENRATH, S., 1968. Estimates of the latent and sensible heat flux for The Caribbean Sea and the Gulf of Mexico. *Limnol. Oceanogr.*, 13, 322–331.

HASTENRATH, S., P. LAMB, 1977. Climatic atlas of the Tropical Atlantic and Eastern Pacific. University of Wisconsin Press.

HASTENRATH, S., 1976. Marine climatology of the Tropical Americas. *Archiv. Meteor. Geophys. Bioklim.*, Ser. B, 24, 1–24.

LETTAU, H., 1939. Bericht über die Dozenten–Afrikareise 1938. Ber. Sächs. Akad. Wiss. Math–Phys. Kl., 15 May. 1939, vol. 91, 119–134.

LIST, R. J., 1968. Smithsonian meteorological tables. Smiths. Miscell. Coll., vol. 114, 6th revised edition, Washington, D. C., 527 pp.

POND, S., D. B. FISSEL, C. A. PAULSON, 1974. A note on bulk aerodynamic coefficients for sensible heat and moisture fluxes. *Boundary–Layer Meteor., 6,* 333–339.

VONDER HAAR, T., J. S. ELLIS, 1974. Atlas of radiation budget measurements from satellites (1962–70). Colorado State University, Department of Atmospheric Science, *Atmospheric Science Paper No. 231,* Fort Collins, Colo., 180 pp.